ELSEVIER

Polymer 41 (2000) 965–973

polymer

Novel cation conductors based on rigid-rod poly(*p*-phenylene)s

Dedicated to Prof Dr Ronald K. Eby, University of Akron, on the occasion of his 70th birthday

P. Baum, W.H. Meyer*, G. Wegner

Max-Planck-Institute for Polymer Research, Ackermannweg 10, P.O. Box 3148, D-55021 Mainz, Germany

Received 24 August 1998; accepted 15 March 1999

Abstract

One approach to combine sufficient ion conductivity and mechanical strength in solid polymer electrolytes (SPE) involves the construction of supramolecular architectures consisting of a liquid-like phase in intimate contact with a rigid phase, both dispersed on a molecular level. Taking advantage of the self-assembling tendencies of poly(*p*-phenylene)s (PPP) as rigid rods, layered structures as reinforcing elements were formed which were separated by a liquid matrix of ethyleneoxide (EO) side chains, in which Lithium salts were dissolved and ion conduction occurs. Single-ion conductors with EO-side chains plus Li-sulfonate groups attached to the PPP backbones exhibit lower conductivities. Although the EO-side chain to Li-sulfonate molar ratio was chosen so that $O/Li^+ \approx 25$, the dc conductivity of such a material was found to be approximately two orders of magnitude lower than in a $PPP(EO)_{5/6}$-Lithium-triflate blend with the same O/Li^+ ratio. The conductivity decreases further when the EO-side chain to sulfonate ratio is decreased. Thus, the increase in the molar concentration of the Li-sulfonate moieties does not lead to higher conductivities either because the number of "free", i.e. mobile, charge carriers is decreased or because the mobility of the ionic species is drastically reduced due to the lack of segmental motion of the matrix. Consequently, when the matrix is plasticized by the addition of large amounts of oligoether, the ionic conductivity increases dramatically and becomes comparable to that of the corresponding multi-ion conducting SPE with the same O/Li^+ ratio.

Keywords: Cation conductors; Poly(*p*-phenylene); Solid polymer electrolytes

1. Introduction

The development of polymeric materials which conduct electricity via the migration of ions has attracted a great deal of attention in recent years [1,2]. Presently, there are many different ion conducting materials described in the literature with the vast majority of them consisting of salts dissolved in a polymer matrix, which generally are known as "solid polymer electrolytes" (SPE), e.g. $LiClO_4$ in polyether matrices [3]. Low molecular weight plasticizers have been added to these polymer–salt complexes to enhance their conductivity. However, the consequent loss of mechanical properties have played a secondary role in most studies in the application of these materials as separators in batteries. Obviously, it is desirable to retain the mechanical strength in these polymer electrolytes which already benefit from typical polymer properties such as ease of processing, flexibility and low specific weight.

Polyelectrolytes in which one type of ionic species is free to migrate while the other is covalently attached to the polymer matrix [4], ensuring that only one ionic species supports conduction, have also been used as ion-conducting materials. This type of ion conductor is especially interesting since the nature of the ion transport can be investigated more thoroughly than in electrolytes with different types of migrating species.

Our approach for the enhancement of the mechanical strength of separators for Lithium batteries is the development of materials based on stiff macromolecules with short flexible ethyleneoxide (EO) side chains. For the present investigations the anionic species are covalently attached to the polymer matrix, ensuring that only the cationic species supports conduction. Here, sulfonate side groups are linked to the polymer backbone to act as counter-ions for the lithium cations which are mobile. These polymers belong to the class of "hairy rod molecules" [5], which have a strong tendency to self-organize into supramolecular architectures when films are cast from solution [6,7,9,10].

The morphology sketched in Fig. 1 indicates how the rigid rod polymers, working as reinforcing elements, together with the flexible EO-side chains, providing the ion-conducting amorphous matrix, combine to enable the production of thin films with high dimensional stability.

* Corresponding author. Tel.: +49-6131-379135; fax: +49-6131-379100.
E-mail address: meyer@mpip-mainz.mpg.de (W.H. Meyer)

0032-3861/00/$ - see front matter
PII: S0032-3861(99)00237-2

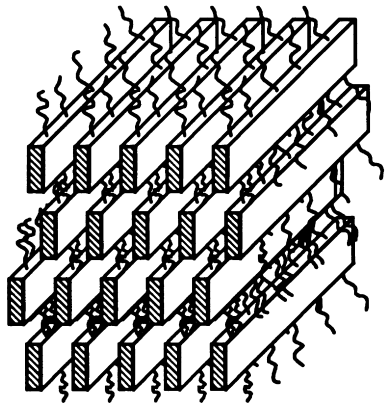

Fig. 1. Schematic of the supramolecular architecture formed by chain stiff macromolecules with flexible side chains (the rods represent the PPP backbones, while the hairs the EO-side chains).

These materials can thus be regarded as "molecular composites" with a dispersion of both components at the molecular level [8–10].

This study reports the use of poly(*p*-phenylenes) (PPP) grafted with both EO-side chains and lithium sulfonates as ion-conducting composites with high dimensional stability. The synthesis, molecular structure, morphology, thermal properties, and the ionic conductivity of these systems are described.

2. Results and discussion

2.1. Synthesis

Integration of the EO-side chains with the sulfonate groups into the rigid polymer backbone required the synthesis of four different monomers. These were composed of three different substituted 2,5-dibromobenzenes **1**–**3** and one unsubstituted *p*-phenylene-bisboronic acid ester **4** as explained in Scheme 1 which shows the synthetic route to the copolymers $PPP[EO]_m[SO_3Li]_n$ [9–11].

The synthesis of the statistical copolymers was carried out via a Suzuki coupling reaction of the type AA/BB using a Pd(0)-catalyst. The polycondensation reaction between the substituted 2,5-dibromobenzenes **1**–**3** and an equimolar quantity of *p*-phenylene-bisboronic acid ester **4**

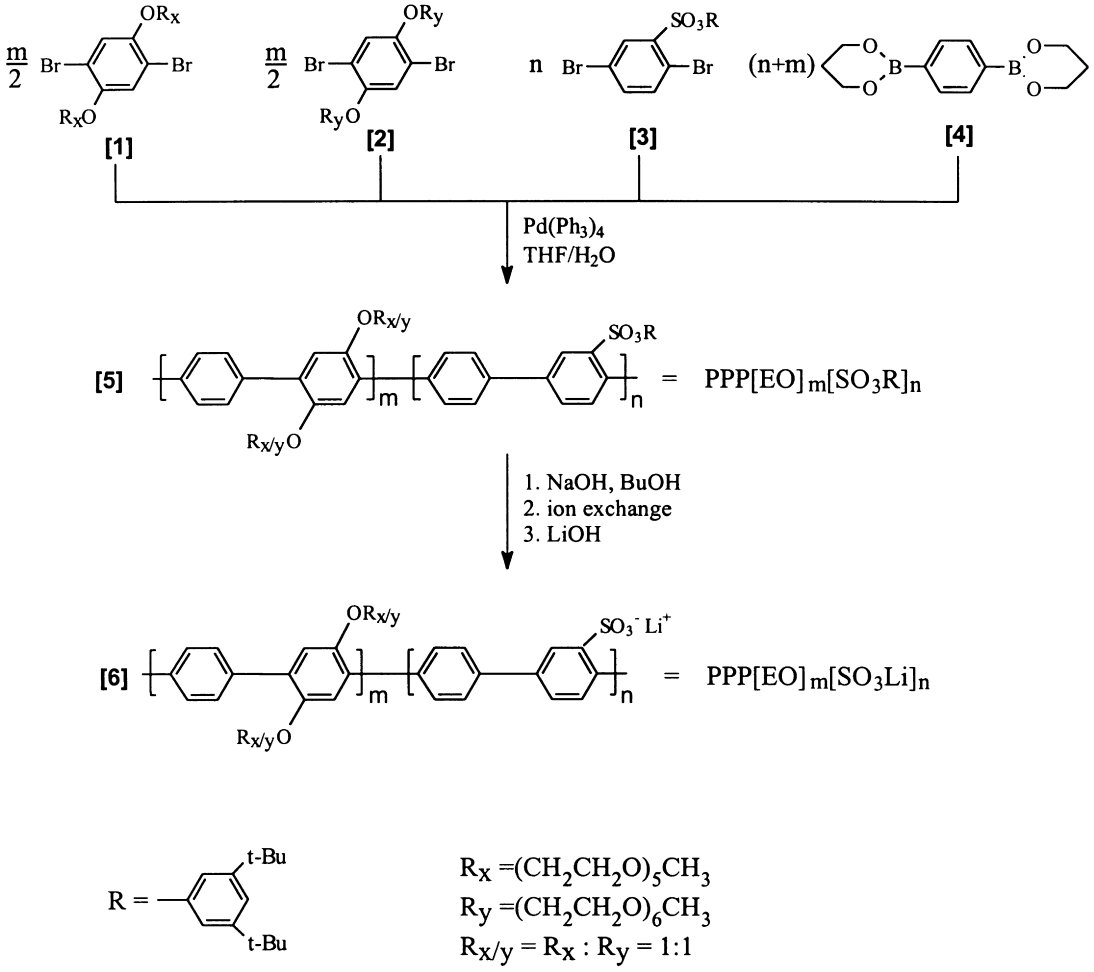

Scheme 1.

Table 1
List of the polymers (see Scheme 1 for the identification of the polymer names) and molecular weight data as determined by SEC and membrane osmometry (MO) for the precursor polymers (X = R) and thermal properties (T_g, ΔC_p) of the polyelectrolytes PPP[EO]$_m$ [SO$_3$Li]$_n$ (X = Li)

Polymer	M_n	M_n^{MO}	Ph_{SEC}[a]	Ph_{MO}[a]	T_g (K)	ΔCp/EO (J/g K)
PPP(EO$_{(1}$(SO$_3$X]$_{0.2}$	5800	9100	18	28	225	6.873×10^{-2}
PPP(EO$_{(1}$(SO$_3$X]$_{0.5}$	7400	15 400	25	51	236	5.951×10^{-2}
PPP(EO$_{(1}$(SO$_3$X]$_{1.4}$	23 800	28 500	89	83	252	6.327×10^{-2}
PPP(EO$_{(1}$(SO$_3$X]$_{2.0}$	19 200	21 100	75	107	–	–
PPP(EO$_{(1}$(SO$_3$X]$_{4.7}$	15 210	31 200	65	133	–	–

[a] Ph represents for the number of phenyl units in the polymer backbone.

was performed in a biphasic THF/aqueous sodium carbonate mixture at 80°C with catalytic amounts of tetrakis-(triphenylphosphine) palladium. The synthetic strategy is outlined in Scheme 1.

End capping reactions were carried out with bromobenzene to remove any free boronic acid end groups that could cause unwanted aggregation.

To suppress the crystallization tendency of the EO-side chains it was necessary to create disorder in the side chain matrix. Therefore, all copolymers consist of equal quantities of **3** and **4** with pentaethyleneglycol and hexaethyleneglycol side chains, respectively. This type of substitution is represented by $R_{x/y}$ with the side chain ratio *x*/*y* kept equal in the present study. The ratio of EO-side chains to sulfonate groups was varied systematically, and is represented by the indices *n* and *m* in the formula PPP[EO]$_m$[SO$_3$R]$_n$ (with *m* set as unity).

The first synthetic step involved the preparation of the polysulfonic esters by coupling the monomers **1**–**4**. This method, using the protected acid groups, was chosen to achieve sufficient solubility for the full characterization of the precursor polymers PPP[EO]$_m$[SO$_3$R]$_n$ **5**. Additionally, the ^{1}H NMR signal of the *tert*-butyl groups of the sulfonic esters allowed the determination of the ratio of the different types of copolymer side groups. Hydrolysis of the precursor polymers occurred after 3 days of treatment with sodium butanolate at about 60°C. The polymers were isolated as sodium salts and then easily converted into the free acids PPP[EO]$_m$[SO$_3$H]$_n$ by ion exchange. The lithium salts PPP[EO]$_m$[SO$_3$Li]$_n$ **6** were then prepared from the free acids by titration with lithium hydroxide (Scheme 1).

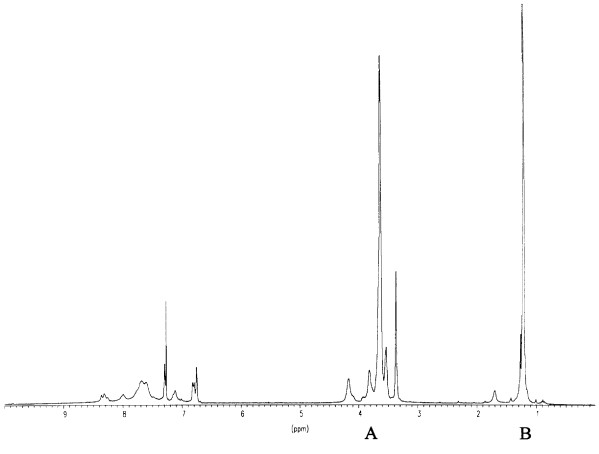

Fig. 2. ^{1}H NMR spectrum of PPP[EO]$_1$[SO$_3$R]$_2$ in CDCl$_3$.

Molecular weight and composition on the precursor polymers as well as thermal data of the corresponding polyelectrolytes are given in Table 1.

2.2. Characterization

2.2.1. Solubility

The precursor polymers PPP[EO]$_m$[SO$_3$R]$_n$ were soluble in organic solvents such as dichloromethane, toluene, and THF, but were insoluble in more polar solvents such as ethanol or water. However, the rigid rod polyelectrolytes PPP[EO]$_m$[SO$_3$Li]$_n$ were insoluble in toluene, THF, chloroform or *N*,*N*-dimethylformamide (DMF), while partly soluble in water and fully soluble in DMSO. This partial solubility allowed characterization by means of ^{1}H and ^{13}C NMR spectroscopies as well as the casting of thin films for dielectric measurements. The solubility of the polymers decreases with both a decrease in the amount of EO-side chains and an increase in the degree of polymerization.

2.2.2. Molecular structure, copolymer composition and polymer morphology

The molecular structure of the polymers was determined on the basis of high resolution ^{1}H and ^{13}C NMR spectra. A typical ^{1}H NMR spectrum of a precursor polymer PPP[EO]$_1$[SO$_3$R]$_2$ is shown in Fig. 2. This spectrum exhibits signals typical of the EO-side chains between $\delta = 3.4$ and 4.2 ppm (A), while the singlet corresponding to the *t*-butyl groups of the sulfonic esters is found at $\delta = 1.2$ ppm (B). As the reactivity of **1** and **2** can be considered as equivalent [9,10], the copolymer composition can be determined by the integral ratios of the respective groups according to the formula $(n/m) = (B/A)(50/18)$, where *A* represents the integral of the EO-side group protons and *B* the integral of the *t*-butyl groups of the sulfonic ester. Additional information of copolymer composition was confirmed by elemental analysis.

By comparing the copolymer composition with the ratio of the monomers, it follows that the sulfonic ester monomer

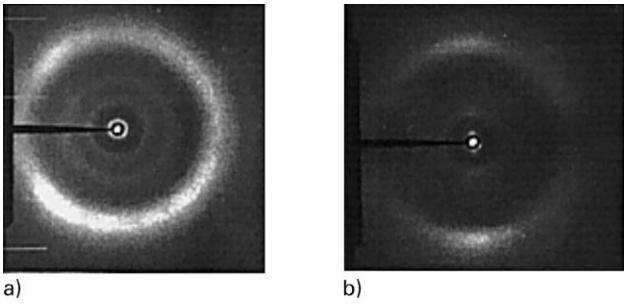

Fig. 3. X-ray diffraction pattern of $PPP[EO]_1[SO_3Li]_{4.7}$ with the incident X-ray beam (a) perpendicular, (b) parallel, respectively, to the film surface.

reacts with a 1.2-fold rate of the monomers carrying the EO-side chains. ^1H NMR also indicated complete polymer hydrolysis by the disappearance of the *t*-butyl-group protons (peak B, Fig. 2).

The morphology of free-standing films cast from solutions of $PPP[EO]_m[SO_3Li]_n$ in DMSO was studied by X-ray diffraction with the incident X-ray beam being parallel and perpendicular to the film surface. In the latter case all polymer salts showed circularly symmetric diffraction. This indicates no in-plane preferential orientation of the polymer chains. However, if the poly-(*p*-phenylene) backbones are arranged parallel to each other in small domains, as can be expected from their liquid-crystalline behavior [11], these domains must be randomly oriented in the film plane.

The spacing of one reflection is consistent with the distance of two phenylene units along the polymer backbone (8.25 Å).

Another reflection at a spacing of 14.52 Å is typical for the packing of the polymer backbones [12]. This indicates that in films of $PPP[EO]_1[SO_3Li]_{0.2}$ and $PPP[EO]_1[SO_3Li]_{0.5}$ there are interdigitating side chains which allow the backbones to achieve a minimum separation of about 14 Å.

The polymers containing a greater EO-side chain content display an additional reflection at $d \cong 22–23$ Å. This is in good agreement with the expected layer separation of oligo(ethylenoxide) substituted poly(*p*-phenylene)s in which no side chain interdigitation occurs [9,10].

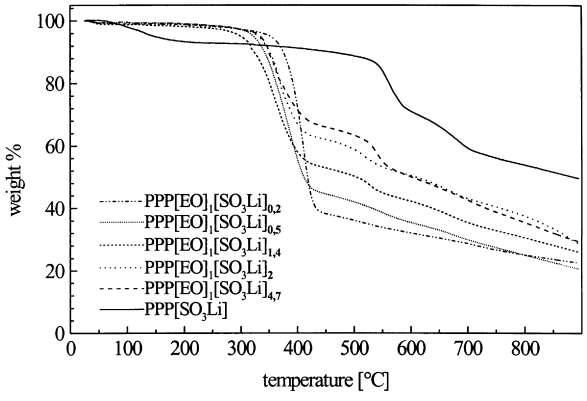

Fig. 4. TGA traces of $PPP[EO]_m[SO_3Li]_n$ under nitrogen (heating rate: 10 K/min).

The diffraction pattern at parallel incidence was anisotropic. The reflection intensities showed sickle-shaped maxima along the meridian and minima along the equator (Fig. 3). These results indicate that the stiff polymer chains are predominantly ordered parallel to the film surface. Ordering increased with increasing sulfonate content and upon annealing.

Light microscopy under crossed polarizers showed that the polymers are lyotropic for $PPP[EO]_m[SO_3R]_n$ in THF and for $PPP[EO]_m[SO_3Li]_n$ in DMSO, respectively.

2.2.3. Molecular weight

The molecular weight of the polymers was determined via size exclusion chromatography (SEC) as well as membrane osmometry (MO) (Table 1). The SEC data were analyzed by using calibration data from sulfonate ester and dodecyl side chain substituted PPP standards [13]. This calibration was necessary, since the hydrodynamic behavior of $PPP[EO]_m[SO_3R]_n$ is presumably different from common standards such as polystyrene.

As seen in Table 1, the MO molecular weights are inconsistent with those obtained via SEC. This discrepancy can be attributed to the use of an absolute method versus a relative method, as well as possible polymer aggregation behavior.

2.2.4. Thermal behavior

Thermogravimetric (TG) measurements of the polyelectrolytes $PPP[EO]_m[SO_3Li]_n$ showed no weight loss below 250°C, while above this temperature three stages of weight loss are observed (Fig. 4). In the range of 250 to 420°C a weight loss consistent with the cleavage of the EO-side chains was observed. Further heating to 480°C displayed a weight loss correlating to loss of the sulfonate salt groups. At 900°C, the weight loss was substantial (20–30%), which indicates pyrolysis of the poly(*p*-phenylene) backbone. TG measurements indicate that the precursor polymers $PPP[EO]_m[SO_3R]_n$ are of about the same thermal stability as the polyelectrolytes $PPP[EO]_m[SO_3Li]_n$. However, they lose most of their weight (35–45%) in one step at about 420°C.

Using differential scanning calorimetry (DSC), a glass transition (T_g) was detected for the three polymers containing the highest amount of EO-side chains. The T_gs increased and broadened as the EO-side chain content was decreased. The change in heat capacity at the glass transition (ΔC_p) can be related to the amount of EO-units ($-CH_2-CH_2-O-$) in the polymer, indicating that the glass transition is an effect of the flexible side chains only (compare Table 1). The observed glass transition temperatures of −48 to −21°C are quite low compared with the T_g of pure poly(ethyleneoxide) of −60°C [2]. This indicates that the side chains have an unexpectedly high mobility even though they are relatively short and fixed at one end.

In the polymers with the two lowest *m*/*n* ratios, $PPP[EO]_1[SO_3Li]_2$ and $PPP[EO]_1[SO_3Li]_{4.7}$, however, no glass transition could be detected. Here, the side chain

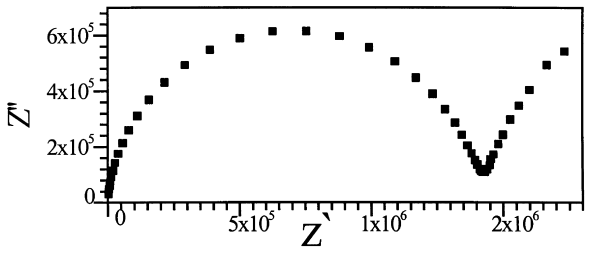

Fig. 5. Cole–Cole plot of $PPP[EO]_1[SO_3Li]_{0.5}$ at 60°C.

density was too low to provide for a detectable mobility increase of the EO-chains.

2.2.5. Dielectric properties

The temperature dependent conductivities of $PPP[EO]_m[SO_3Li]_n$ were obtained from impedance spectroscopy of cast films, sandwiched between two blocking gold electrodes. From a complex impedance plot (Fig. 5) the effective dc resistance R was obtained by reading Z' at minimum Z''.

The DC conductivity σ_{DC} is related to the dc resistance R as $\sigma_{DC}(T) = (d/R(T)A)$ (with d = distance between the electrodes, A = area of the electrodes.) $PPP[EO]_m[SO_3Li]_n$ conductivities are shown in Fig. 6.

To serve as a basis of comparison, the conductivities of a sulfonate-free PPP containing only EO-side chains (PPP[EO]) and an EO-side-chain-free PPP containing only sulfonate groups ($PPP[SO_3Li]$) are included in Fig. 6. The former was doped with Lithium trifluoromethanesulfonate (CF_3SO_3Li) in a O/Li^+ molar ratio of 50.

The data in Fig. 6 were fit using the Williams–Landel–Ferry (WLF) equation [14]

$$\sigma(T) = \sigma_0 \exp\left[\frac{C_1(T - T_g)}{C_2 + T - T_g}\right],$$

where T_g is the glass transition temperature (taken from DSC measurements), σ_0 is the conductivity at $T = T_g$ and C_1 and C_2 are constants. σ_0, C_1 and C_2 were allowed to vary

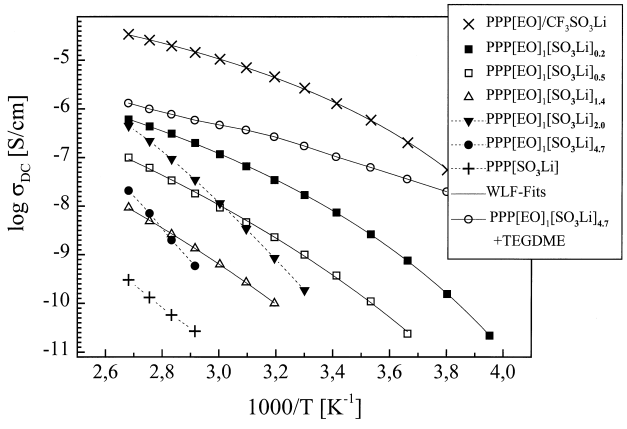

Fig. 6. Ion conductivities vs. T^{-1} for $PPP[EO]_m[SO_3Li]_n$, PPP[EO]/CF_3SO_3Li, $PPP[SO_3Li]$ and $PPP[EO]_1[SO_3Li]_{4.7}$ plasticized with 72 wt.% TEGDME.

while holding T_g constant. A compilation of the WLF fitting parameters for $PPP[EO]_m[SO_3Li]_n$is displayed in Table 2.

Fig. 6 shows that the conductivity first decreases with an increase in the density of Li-sulfonate, thus with increasing amount of available lithium ions. Further, the conductivity of the polymers $PPP[EO]_m[SO_3Li]_n$ is, in general, lower than the conductivity of the corresponding PPP[EO]/CF_3SO_3Li mixtures, but higher than the conductivity of $PPP[SO_3Li]$ without any EO-side chains. However, the different slopes for the group of polymers PPP[EO], $PPP[EO]_1[SO_3Li]_{0.2}$, $PPP[EO]_1[SO_3Li]_{0.5}$ and $PPP[EO]_1[SO_3Li]_{1.4}$ in comparison to the slopes of the group of polymers $PPP[EO]_1[SO_3Li]_2$, $PPP[EO]_1[SO_3Li]_{4.7}$ and $PPP[SO_3Li]$ were unexpected. As the slope in the Arrhenius plot in Fig. 6 corresponds to the activation energy of the conductivity, this indicates differences in the conductivity mechanisms between the two groups of polymers.

To understand these results fully, one must consider that the relative amount of EO-side chains decreases with a simultaneous increase in the number of moles Li^+ per mole of polymer (Table 3). However, as the side chains form the ion-conducting amorphous matrix, the relative number of side chain oxygens per lithium cations may be of paramount importance for the conduction mechanism. As can be seen from Table 3, the O/Li^+ ratio, i.e. the number of available coordination sites for a Li^+ in the side chain matrix, decreases from 66.7 in $PPP[EO]_1[SO_3Li]_{0.2}$ to 2.7 in $PPP[EO]_1[SO_3Li]_{4.7}$. When comparing Fig. 6 and Table 3 it becomes evident that down to a O/Li^+ ratio of about 10 the conductivity decreases continuously, while the slope of the WLF fits remains more or less unchanged (with a small tendency to increase). At a O/Li^+ ratio of 6.5 and lower, however, the conductivity behavior of $PPP[EO]_1[SO_3Li]_2$ and $PPP[EO]_1[SO_3Li]_{4.7}$ becomes more temperature sensitive. The temperature dependence approximates that of the polyelectrolyte without EO-side chains ($O/Li^+ = 0$, $PPP[SO_3Li]$).

As conductivity depends on both the number of free charge carriers (N) and their mobility (μ), we consider both to help explain the conductivity behavior of these polyelectrolytes. N depends on the number and degree of dissociation of the SO_3Li-groups in our polymers, which are not only a function of the O/Li^+-ratio but may also depend on the number and length of side chains per polymer repeat. Thus, with decreasing O/Li^+-ratio a reduction in the dissociation of the sulfonate groups can be expected. In contrast, μ depends on the molecular composition through T_g which is sensitive to O/Li^+. As T_g increases with decreasing O/Li^+-ratio, a reduction in the mobility can be expected. To differentiate between the effect of reduced N and reduced μ, and especially to explain the change in mechanism, more detailed experiments are necessary.

The addition of TEGDME (tetraethylene-glycol-dimethylether) to $PPP[EO]_1[SO_3Li]_{4.7}$, which increases the O/Li^+-ratio from 2.7 to 25.0, causes a dramatic increase in conductivity. To our own surprise, the conductivity in

Table 2
WLF parameters used for fitting the conductivity data in Fig. 6

Polymer	WLF parameter			
	C_1	C_2 (K)	T_g (K)	log σ_0 (S/cm)
PPP[EO]/CF_3SO_3Li	26.97	27.06	220	− 14.43
$PPP[EO]_1[SO_3Li]_{0.2}$	26.74	46.10	225	− 15.07
$PPP[EO]_1[SO_3Li]_{0.5}$	26.29	86.24	236	− 14.05
$PPP[EO]_1[SO_3Li]_{1.4}$	26.87	108.98	252	− 14.19

$PPP[EO]_1[SO_3Li]_{4.7}$ plasticized with 72 wt.% TEGDME even exceeded the level of $PPP[EO]_1[SO_3Li]_{0.2}$ with a O/Li^+ ratio of 66.7. Based on an O/Li^+-ratio increase alone, a conductivity comparable to $PPP[EO]_1[SO_3Li]_{0.5}$ was expected. However, in contrast to the backbone-attached EO-side chains, the mobile TEGDME molecules in the side chain matrix can support the Lithium-ion transport by diffusion. This effect may explain the unexpectedly high conductivity increase in plasticized $PPP[EO]_1[SO_3Li]_{4.7}$ materials.

Surprisingly, the addition of large quantities of plasticizer does not lead to liquid-like materials, but films prepared from $PPP[EO]_1[SO_3Li]_{4.7}$ plasticized with 72 wt.% TEGDME are not even tacky and exhibit surprisingly good mechanical properties. This appears to be the result of the reinforcing nature of the rigid polymer backbones which demonstrates the concept of the molecular composite-based polyelectrolyte as a possible separator for batteries.

3. Experimental section

3.1. Measurements

^1H and ^{13}C NMR data were obtained with a Bruker AC 300 (300 MHz) spectrometer using $CDCl_3$ as the chemical shift standard. FT-IR spectra were recorded on a Perkin–Elmer Paragon 1000 spectrometer. Mass spectra were obtained from a VG-Biotech Trio-2000 instrument with EI ionization (70 eV). The morphology of the solution-cast films was characterized by X-ray diffraction using a flat-film camera with Ni-filtered CuK_α radiation. Thermogravimetry was performed on a Mettler TG 50 with a heating rate of 10 K/min. DSC measurements were carried out under nitrogen with a heating rate of 10 K/min on a Mettler DS TA 3000 instrument; glass transition temperatures (T_gs) were taken at the inflection points of the ΔC_p steps. Ion conductivities of polymer electrolytes were determined using a Schlumberger SI 1260 impedance/gain phase analyzer with a custom-built dielectric interface with a frequency range of $0.1–10^5$ Hz. The measurements were performed in a Novocontrol cryostat. The sample temperature was regulated by a temperature-controlled nitrogen gas jet and measured with a platinum resistor (Pt 100) inserted in one electrode. For sample preparation, polymers were dissolved in DMSO and cast onto gold electrodes. After evaporation of the solvent under vacuum the films were vacuum dried at 70–80°C for at least 24 h. In order to provide good electrode contact, the gold counter-electrode was vapor-deposited onto the polymer film. The dc conductivities obtained from Cole–Cole plots (Z'' versus Z') were identical with the low frequency plateau of the ac conductivities.

Table 3
O/Li^+-ratio in the polymers $PPP[EO]_m[SO_3Li]_n$, PPP [EO]/CF_3SO_3Li and $PPP[SO_3Li]$ for comparison

No.	Polymer	O/Li^+-ratio[a]	mole Li^+ per mole polymer[b]
1	PPP[EO]/CF_3SO_3Li	50.0	0.26
2	$PPP[EO]_1[SO_3Li]_{0.2}$	66.7	0.17
3	$PPP[EO]_1[SO_3Li]_{0.5}$	25.6	0.33
4	$PPP[EO]_1[SO_3Li]_{1.4}$	9.3	0.58
5	$PPP[EO]_1[SO_3Li]_2$	6.5	0.66
6	$PPP[EO]_1[SO_3Li]_{4.7}$	2.7	0.82
7	$PPP[EO]_1[SO_3Li]_{4.7}$ + 72 wt.% TEGDME	25.0	–
8	$PPP[SO_3Li]$	0	1

[a] O includes only the oxygens of the EO-side chains and that of TEGDME.

Table 4
Elemental analysis of $PPP[EO]_m[SO_3R]_n$

Polymer	Calculated (wt.%)				Found (wt.%)		
	C	H	S	O	C	H	S
$PPP[EO]_1[SO_3R]_{0.2}$	63.37	7.95	0.82	27.86	62.94	7.86	0.79
$PPP[EO]_1[SO_3R]_{0.5}$	64.88	7.78	1.77	25.57	64.93	7.72	1.69
$PPP[EO]_1[SO_3R]_{1.4}$	67.64	7.46	3.49	21.41	66.32	7.62	3.40
$PPP[EO]_1[SO_3R]_{2.0}$	68.73	7.34	4.17	19.77	68.56	7.28	4.23
$PPP[EO]_1[SO_3R]_{4.7}$	71.07	7.07	5.64	16.22	70.64	7.01	5.56

3.2. Materials

All reagents were purchased from Merck, Fluka, or Aldrich and were used without further purification unless otherwise stated. In order to remove peroxide impurities and oxygen, the THF for polymerization reactions was refluxed with a sodium/potassium alloy and distilled under argon. Oxygen-free water for the polymerization procedure was prepared by distilling under argon followed by purging with a nitrogen stream for at least 3 h. The monomers

Table 5
Solvent mixtures for the polymeric sulfonates

Polymer	Solvent mixtures
$PPP[EO]_1[SO_3Na]_{0.2}$	THF/H_2O
$PPP[EO]_1[SO_3Na]_{0.5}$	$EtOH/H_2O$
$PPP[EO]_1[SO_3Na]_{1.4}$	THF/H_2O
$PPP[EO]_1[SO_3Na]_{2.0}$	CH_3CN/H_2O
$PPP[EO]_1[SO_3Na]_{4.7}$	THF/H_2O

p-phenylene-bisboronic acid ester [15] **4**, 2,5-dibromo-1,4-bis(pentakis(oxyethylene))benzene [9,10] **1**, 2,5-dibromo-1,4-bis(hexakis-(oxyethylene))benzene [9,10] **2** and 2,5-dibromoarylsulfon esters [11] **3** were prepared as described in the literature. The preparation of the polymerization catalyst tetrakis-(triphenylphosphine)-palladium was carried out according to the literature [16].

3.3. Synthesis of precursor polymers $PPP[EO]_m[SO_3R]_n$

Equimolar amounts of *p*-phenylene-bisboronic acid ester **4** and the sum of the three dibromides 2,5-dibromo-1,4-bis(pentakis(oxyethylene))benzene **1**, 2,5-dibromo-1,4-bis(hexakis(oxyethylene))-benzene **2** and 2,5-dibromoarylsulfonic ester **3** are dissolved in a mixture of absolute THF and water under argon atmosphere. A concentration of 170 ml THF/water was used for every millimole of the bisboronic acid ester **4**. $NaHCO_3$ was added to the reaction mixture until a concentration of 2 M was reached followed by the addition of 5×10^{-3} equivalent of the palladium catalyst $Ph[PPh_3]_4$. The ratio of the dibromides **1** and **2** was kept 1:1 in order to incorporate equal amounts of pentaethyleneglycol and hexaethyleneglycol side chains into the polymer. Care must be taken to exclude oxygen from the reaction mixture and to protect the reaction vessel from sunlight as the palladium catalyst is oxygen and light sensitive. Bromobenzene (0.01 mol equivalent) was added after stirring the reaction mixture at 80°C for 3 days. The polymerization was terminated after 4 days by precipitating the THF/polymer solution into a fivefold volume of petroleum ether. The precipitate was filtered and washed with water.

Reprecipitation was carried out from toluene for $PPP[EO]_1[SO_3R]_{1.4}$, $PPP[EO]_1[SO_3R]_2$ and $PPP[EO]_1[SO_3R]_{4.7}$ and dichloromethane for $PPP[EO]_1[SO_3R]_{0.2}$ and $PPP[EO]_1[SO_3R]_{0.5}$, respectively. The dissolved polymers were subsequently filtered over silica gel. After precipitation in petroleum ether and vacuum drying at 50°C the pure product was recovered at yields of 80–95%.

Characteristic data of the precursor polymers

1. $PPP[EO]_1[SO_3R]_2$

^{1}H NMR($CDCl_3$): $\delta = 8.3$ (m, 2H, H^2), 8.0 (m, 2H, H^6), 7.7, 7.6 (m, 14H, H^8, H^9, H^5, H^{22}, $H^{22\prime}$, H^{23}, $H^{23\prime}$), 7.29 (m, 2H, H^{14}), 7.1 (m, 2H, H^{18}, $H^{18\prime}$), 6.8 (s, 4H, H^{12}), 4.2 (m, 4H, H^{25}, $H^{25\prime}$), 3.8 (m, 4H, H^{26}, $H^{26\prime}$), 3.6 (m, 32H, H^{27}, $H^{27\prime}$, H^{28}, $H^{28\prime}$), 3.5 (m, 4H, H^{29}, $H^{29\prime}$), 3.4 (m, 6H, H^{30}, $H^{30\prime}$), 1.21 (s, 18H, H^{16}) ppm (Fig. 2).

^{13}C NMR($CDCl_3$): $\delta = 152.8$ (C^{13}), 150.7 (C^{19},$C^{19\prime}$), 149.8, 149.3 (C^{11}, isomers), 140.5–138.5 (C^7, C^{10}, C^{21}, $C^{21\prime}$, C^{24}, $C^{24\prime}$), 135.3, 135.0, 133.9, 133.6, 133.5, (C^1, C^3, C^4, C^{17}, $C^{17\prime}$, C^{20}, $C^{20\prime}$, isomers), 131.7, 130.4, 129.6, 129.2, 128.9, 128.0, 127.8, 126.8, 126.4 (C^2, C^5, C^6, C^8, C^9, C^{22}, $C^{22\prime}$, C^{23}, $C^{23\prime}$ isomers), 121.0 (C^{14}), 117.1 (C^{18}, $C^{18\prime}$), 116.5 (C^{12}), 72.0 (C^{25}, $C^{25\prime}$), 71.2, 71.0, 70.9, 70.7, 70.6, 70.3, 69.9, 69.8, 69.7, 69.5 (C^{26}, $C^{26\prime}$, C^{27}, $C^{27\prime}$, C^{28}, $C^{28\prime}$, C^{29}, $C^{29\prime}$), 59.0 (C^{30}, $C^{30\prime}$), 35.0 (C^{15}), 31.3 (C^{16}) ppm.

For the elemental analysis of the polymers $PPP[EO]_m$-$[SO_3R]_n$ see Table 4.

3.4. Synthesis of the polymers $PPP[EO]_m[SO_3Li]_n$

Sodium butanolate solution was prepared by dissolving NaOH in 1-butanol. To a solution of 5 g precursor polymer $PPP[EO]_m[SO_3R]_n$ in 150–350 ml of toluene a threefold molar excess of sodium butanolate solution was added dropwise over a period of 1/2 h. During this process the reaction mixture was kept under nitrogen atmosphere. After further stirring for 48 h, the reaction mixture was neutralized with $NaHCO_3$. The product was filtered and washed with toluene and water to remove phenol residues. The product was isolated after freeze drying as a pale gray solid.

If the resulting sulfonate failed to precipitate out of the reaction mixture the polymer product was obtained by pouring the reaction mixture into an excess of petroleum ether.

When the resulting products were not completely saponified (according to ^{1}H NMR they contain still 1–7% unsaponified ester groups), a second saponification in ethanol was required.

To convert the sodium salt into the free sulfonic acid and to remove foreign salts, the polymeric sulfonate was dissolved in a solvent/water mixture (Table 5) and acidified

1 **$PPP[EO]_1[SO_3R]_2$**

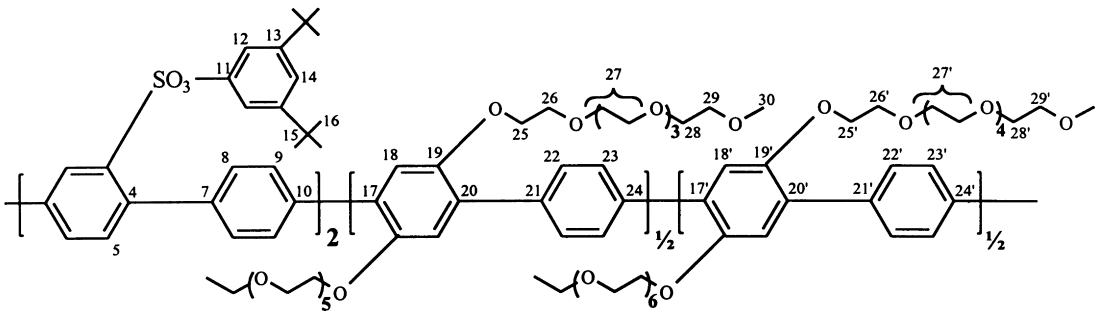

Table 6
FT-IR data

Polymer	$\nu(CH_2, CH_3)$	$\nu^a(SO_3\_M^+)$	$\omega(CH_2)$		$\nu(SO_3\_M^+)$		$\nu^s(SO_3\_M^+)$	Unidentified	δ(Ar–CH)
$PPP[EO]_1[SO_3Li]_{0.2}$	2872.4	1472.7	1387.7	1352.1	1249.9	1215.4	1109.9	1064.4	947.5
$PPP[EO]_1[SO_3Li]_{0.5}$	2873.1	1470.6	1387.5	1284.8	1244.2	1212.3	1105.3	1064.0	947.1
$PPP[EO]_1[SO_3Li]_{1.4}$	2873.8	1469.1	1385.0	1352.2	1240.6	1204.3	1099.8	1064.1	947.2
$PPP[EO]_1[SO_3Li]_{2.0}$	2374.1	1468.8	1383.0	1351.9	1238.1	1204.4	1099.2	1064.3	947.4
$PPP[EO]_1[SO_3Li]_{4.7}$	2876.9	1468.1	1379.8	1352.4	1229.7	1204.6	1098.8	1064.6	948.8

with concentrated HCl. The solution was then passed through a column filled with an amberlist ion exchange resin in protonated form. After solvent removal the product was freeze dried from water.

The lithium salts $PPP[EO]_m[SO_3Li]_n$ **6** could be prepared from the free acids by titration with lithium hydroxide.

For the FT-IR data see Table 6.

Characteristic data of the polyelectrolytes

2. $PPP[EO]_1[SO_3H]_2$

2 $PPP[EO]_1[SO_3H]_2$

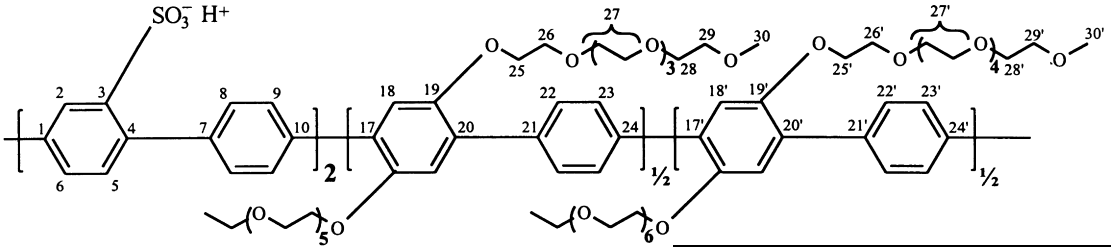

^{1}H NMR(DMSO): $\delta = 8.4$ (m, 2H, H^2), 7.7, 7.6 (m, 14H, H^8, H^6, H^5, H^{22}, $H^{22\prime}$, H^{23}, $H^{23\prime}$), 7.3 (m, 2H, H^5), 7.2 (m, 2H, H^{18}, $H^{18\prime}$), 6.8 (s, 4H, H^{12}), 4.2 (m, 4H, H^{25}, $H^{25\prime}$), 3.8 (m, 4H, H^{26}, $H^{26\prime}$), 3.5 (m, 32H, H^{27}, $H^{27\prime}$, H^{28}, $H^{28\prime}$), 3.4 (m, 4H, H^{29}, $H^{29\prime}$), 3.4 (m, 6H, H^{30}, $H^{28\prime}$) ppm.

^{13}C NMR(DMSO): $\delta \approx 150$ (C^{19},$C^{19\prime}$), 140.5–138.5 (C^7, C^{10}, C^{21}, $C^{21\prime}$, C^{24}, $C^{24\prime}$), 135–133 (C^1, C^3, C^4, C^{17}, $C^{17\prime}$, C^{20}, $C^{20\prime}$, isomers), 130.5, 130.4, 129.9, 129.2, 128.9, 128.3, 126.6, 125.6, 124.4 (C^2, C^5, C^6, C^8, C^9, C^{22}, $C^{22\prime}$, C^{23}, $C^{23\prime}$ isomers), 117.2 (C^{18}, $C^{18\prime}$), 72.0 (C^{25}, $C^{25\prime}$), 70.9, 69.6, 69.4, 69.2, 68.8 (C^{26}, $C^{26\prime}$, C^{27}, $C^{27\prime}$,C^{28}, $C^{28\prime}$, C^{29}, $C^{29\prime}$), 57.5 (C^{30}, $C^{30\prime}$) ppm.

4. Conclusions

The concept of a rigid-rod scaffolding to provide enhanced mechanical stability in intimate contact with a liquid-like matrix to facilitate ion conduction is demonstrated. If the anions are fixed to the polymer as in cationic polyelectrolytes, the conductivity usually appears to be some orders of magnitude lower in comparison with polymer electrolytes, in which both cations and anions can contribute to the charge transport. The present study demonstrates, however, that the conductivity dependence on relative cation concentration (O/Li^+-ratio) cannot simply be explained by the effective number of charge carriers, and that the ion mobility must be taken into account. Thus, if the mobility is increased by the addition of a plasticizer so that the O/Li^+-ratio is sufficiently increased, conductivities comparable to multi-ion conductors are obtained.

Acknowledgements

Financial support from BMBF (Förderkennzeichen 03N3007B9) is gratefully acknowledged. The authors thank Christian Honeker for editing the manuscript.

References

[1] MacCallum JR, Vincent CA. Polymer Electrolyte Reviews 2. London: Elsevier Applied Science, 1989.
[2] Gray F. Polymer Electrolytes, RSC Materials Monographs. Cambridge: Royal Society of Chemistry, 1997.
[3] Meyer WH. Adv Mater 1998;10(6):439.
[4] Hardy LC, Shriver DF. J Am Chem Soc 1985;107:3823.
[5] Ballauf M. Angew. Chem Int Ed Engl 1989;28:253.
[6] Wegner G. Thin Solid Films 1992;216:105.
[7] Helmer-Metzmann F, Ballauf M, Schulz RC, Wegner G. Makromol Chem 1983;190:985.
[8] Krause SJ, Haddock TB, Price GE, Adams WW. Polymer 1988;29:195.
[9] Lauter U, Meyer WH, Wegner G. Macromolecules 1997;30(7): 2092–2101.
[10] Lauter U, Meyer WH, Enkelmann V, Wegner G. Macromol Chem Phys 1998;199:2129–2140.

[11] Rulkens R, Schulze M, Wegner G. Macromol Rapid Commun 1994;15:669–676.
[12] M. Remmers, Dissertation, Mainz, 1996.
[13] Vanhee S, Rulkens R, Lehmann U, Rosenauer C, Schulze M, Köhler W, Wegner G. Macromolecules 1996;29(15):5136.
[14] Stroebel GR. The Physics of Polymers. Berlin: Springer, 1996.
[15] Ciferri A. Polym Engng Sci 1994;44:59.
[16] Coulson DR, et al. Inorg Synth 1972;13:121–123.